EFFECT OF A CONSTANT HEAT SOURCE ON EVAPORATIVE INSTABILITY IN A SOLID-LIQUID-VAPOR SYSTEM

by

Aslı Karaçelik

B.S., Chemical Engineering, Yeditepe University, 2012

Submitted to the Institute for Graduate Studies in
Science and Engineering in partial fulfillment of
the requirements for the degree of
Master of Science

Graduate Program in Chemical Engineering

Boğaziçi University

2014

EFFECT OF A CONSTANT HEAT SOURCE ON EVAPORATIVE INSTABILITY IN A SOLID-LIQUID-VAPOR SYSTEM

APPROVED BY:

Title and Name of Supervisor .....
(Thesis Supervisor)

Title and Name of Examiner .....

Title and Name of Examiner .....

DATE OF APPROVAL: Day.Month.Year

ACKNOWLEDGEMENTS

Foremost, I would like to render thanks to Assoc. Prof. Kerem Uguz for his boost, heartening and guidance. His thirst for knowledge and meritorious conduct were inspirational to me. I also would like to express thanks to Prof. Ranga Narayanan for his advice and keen attentiveness. I have admired his avidity to his work.

I would like to express my heart-felt thanks to my beautiful family for their endless love and moral support. I feel so lucky that I have such a lovely family.

Many thanks go to my old friends, Cumhur Boyraz, Burcu Kandira, Gonul Aykulug, Zeynep Aslan, Ayse Kavukcu and Olcay Seval for their encouragement and friendship. They will always be with me all through my life.

Special thanks go to Meltem Macit, Ezgi Yildiz and Zeynep Percin for making me tenacious and spirited. We will be always together wherever we are.

Aycan Hacioglu, Kyle Edwin and Brad Messmer thank you a lot for being in my life. Aycan, you are the most benevolent person I have ever met. Thank you wholeheartedly for everything you have done for me. Kyle, you have succoured me whenever I need and I know you will always be there. It was a big chance to meet with all of you. I also want to express thanks to Xin Lin and Erdem Uguz for helping me in Gainesville in every respect.

I would also like to express gratitude to the financial support for this thesis provided by the Marie Curie IRSES Fellowship within the 7th European Community Framework Programme Project Patterns and Surfaces Grant 269207.

ABSTRACT

EFFECT OF A CONSTANT HEAT SOURCE ON EVAPORATIVE INSTABILITY IN A SOLID-LIQUID-VAPOR SYSTEM

When a liquid underlies its own vapor, convection may arise due to evaporation without gravity or surface tension gradient effects. This process is named as pure evaporative convection. In this study, standard linear stability of a solid-liquid-vapor system considering an evaporative liquid into its own vapor is investigated. A constant heat source is considered in the solid part of the system and the effect of that heat source on the linear stability is studied. Inputs to the system are the constant heat, the depths of the solid, the liquid and the vapor and the physical parameters, which are assumed to be constant while the output is the temperature difference at which convection starts. The aim is to parametrically analyze this system and compare it with a liquid-vapor system where the bottom plate is kept at constant hot and upper plate at constant low temperature. In the study, the effect of the heat source number, which appears in the energy balance equation for the solid part, the solid depth, the liquid and the vapor flows on the critical evaporation number and dispersion curve are examined. It is concluded that the vapor flow stabilizes the system while the heat source number, the liquid flow and the solid depth destabilize the system.

ÖZET

KATI-SIVI-BUHAR SİSTEMİNDE SABİT ISI VEREN KAYNAĞIN BUHARLAŞMA NEDENİYLE OLUŞAN KARARSIZLIK ÜZERİNDEKİ ETKİSİ

Bir sıvı kendi buharının altındayken, konveksiyon, yer çekimi ve yüzey gerilimi değişimi olmadan buharlaşma nedeniyle oluşabilir. Bu süreç sadece buharlaşmayla meydana gelen konveksiyon olarak adlandırılır. Bu çalışmada, katı-sıvı-buhar sisteminin buharlaşabilen bir sıvı ve onun kendi buharı düşünülerek standart lineer stabilitesi incelenmiştir. Sistemin katı bölümünde sabit bir ısı kaynağı düşünülmüştür ve bu ısı kaynağının lineer stabilite üzerindeki etkisi araştırılmıştır. Sistemin girdileri sabit kabul edilen ısı, katı, sıvı ve buharın derinlikleri ve fiziksel parametrelerdir, dışarı verilen ise konveksiyonun başladığı sıcaklık farkıdır. Amaç bu sistemi parametrik olarak analiz etmek ve onu alttaki plakanın sıcak olarak sabit tutulduğu ve üstteki plakanın daha düşük sıcaklıkta sabit tutulduğu sıvı-buhar sistemiyle karşılaştırmaktır. Çalışmada, katı bölüm için enerji korunumu denkleminde gözüken ısı kaynağı sayısının, katı derinliğinin, sıvı ve buhar akışının kritik buharlaşma sayısı üzerindeki etkisi incelenmiştir. Buhar akışı sistemi kararlı hale getirirken, ısı kaynağı sayısının ve sıvı akışının sistemi kararsızlaştırdığı sonucuna varılmıştır.

TABLE OF CONTENTS

LIST OF FIGURES

LIST OF SYMBOLS

$C_{P_{G,L,S}}$	Heat capacity of the vapor, the liquid and the solid
$\hat{G}_{G,L}$	Gibbs free energy per unit mass for the vapor and the liquid
H	The surface mean curvature
$\hat{H}_{G,L}$	Enthalpy per unit mass for the vapor and the liquid
$H_{G,L,S}$	The vapor, the liquid and the solid depth
$\mathbf{i}$	Unit vector in the x direction
$\mathbf{I}$	Identity tensor
k	Wavenumber
$k_{G,L,S}$	Thermal conductivity of the vapor, the liquid and the solid
$\mathbf{n}$	Unit outward normal vector
$p_{G,L}$	Pressure of the vapor and the liquid
$\mathbf{q}_{G,L}$	Heat flux vector for the vapor and the liquid
$\hat{Q}_S$	Mass rate of thermal energy production in the solid
$\mathbf{S}_{G,L}$	Deviatoric part of the stress tensor for the vapor and the liquid
$\hat{S}_{G,L}$	Entropy per unit mass for the vapor and the liquid
$\mathbf{t}$	Unit tangent vector
$\mathbf{T}_{G,L}$	Total stress tensor for the vapor and the liquid
$T_{G,L,S}$	Temperature of the vapor, the liquid and the solid
$\hat{U}_{G,L}$	Internal energy per unit mass for the vapor and the liquid
$\mathbf{v}_{G,L}$	Velocity vector of the vapor and the liquid
$\hat{V}_L$	Volume per unit mass for the liquid
Z	Interface shape
γ	Interfacial tension
κ_S	Themal diffusivity of the solid
$\mu_{G,L}$	Viscosity of the vapor and the liquid
$\nu_{G,L}$	Kinematic viscosity of the vapor and the liquid
σ	Growth rate
$\rho_{G,L,S}$	Density of the vapor and the liquid

$\mathcal{L}$	Latent heat of evaporation

LIST OF ACRONYMS/ABBREVIATIONS

Ca	Capillary number
E	Evaporation number
Pr	Prandtl number

1. INTRODUCTION

Evaporation and condensation are simply the change of liquid to the vapor state and vice versa by using energy. This phenomenon may bring about an interfacial instability when the temperature drop goes beyond a critical value [1]. The abrupt waviness of the previously flat surface at the interface describes this instability which affect the final state of a product [2]. Many technologies such as the glass fabrication, surface coating, the dry-eye syndrome, the drying of lake beds, thin-film evaporators and heat pipe technology involve the evaporation process. In most of these applications, evaporation occurs with concentration gradient or temperature gradient or both. Merely, the temperature gradient is taken into account in this study.

Previously, it was thought that the vapor does not affect the interfacial instability. Initially, the model that does not contain the vapor dynamics was used in the previous study of Burelbach *et al.* [3]. They studied the effects of the mass transfer rate in the absence of thermodynamic equilibrium at the interface in thermocapillary, vapour recoil, and rupture using non-linear instabilities. In the study, horizontal liquid layers between the plates were used. The interface shape was obtained by long-wave evolution equations. Recently, Oron [4] and Margerit *et al.* [5] used the same concept in their systems. Margerit *et al.* analyzed their systems with 1.5 sided model. Liquid dynamics and diffusion in the vapor is taken into consideration in this type of model.

There are three mechanisms that drive the convection: Rayleigh convection, Marangoni convection and pure evaporation. Rayleigh convection which is also called natural convection ensued from the density variation with respect to temperature in a gravitational field. In Marangoni convection, variation of the surface tension with temperature comes into the picture and it can occur without a gravitational field. Initially, Pearson [6] expounded the effect of surface tension on cells stated in Bénard's study and found that the surface tension causes cellular motion. The physics of the problem convolutes if all the effects are incorporated even for a single-component system. In this study, pure evaporation is taken into account for a pure liquid which contacts its

own vapor in the absence of gravity and surface tension gradient. The best way to acquire the gist of evaporative instability is neglecting all the effects such as gravity, surface tension etc. and considering an evaporative liquid underlying its own vapor.

Fluid mechanics in the vapor phase is included in recent studies. Haut and Colinet [7] investigated the effect of inert gas on Bénard instability which arises due to surface tension in a system that liquid contacts its own vapor. They found that the existence of inert gas improves the Bénard instability and comprehended that the two layer system could be turned into a one layer system when the liquid layer is thin enough. In addition, they introduced the heat transfer coefficient by using Biot number at the liquid-vapor interface. Ozen and Narayanan [8] used the linear stability method to discern the effect of evaporative instability at the interface for finite vapor depth. They concluded that the vapor flow stabilizes the system and liquid flow has counterproductive effect on stability. In their another study, they also collate the pure marangoni with pure evaporation problem. The disparity between these two problems is that the vapor has stabilizing effect and the transverse diffusion makes the crests and troughs more wavy on pure evaporation problem. McFadden *et al.* [9] canvassed the effect of entropy for the two phase system. They deduced that when the entropy of the system dwindles, Marangoni effect mounts up in the system. Marangoni effect may not come into being due to high pressure gradient with respect to the temperature. That is to say that isothermal behavior of the system does not change; hence there will be no driving force to be able to observe Marangoni effect. Huang and Joseph [10] used incompressible pure liquid surmounted by its own vapor. In the system, even though there was no convection, phase change appeared. They construed this phenomenon as the condition of the temperature continuity could not be used when high temperature difference is applied to the system. When the interface attains the saturation temperature, they considered that there is no thermodynamic equilibrium at the interface. Therefore, they used temperature discontinuity condition at the interface.

Figure 1.1 depicts the physical system of the study. There are three phases in the system: solid, liquid and vapor. The solid part is taken to be copper as it is a widely known conductive metal and water which contacts with its own vapor is taken as to be

the liquid. Straight, dashed wave lines and arrays in the figure present the base, the perturbed states and liquid-vapor motion owing to local evaporation and condensation, respectively.The input variables are the constant physical properties, the fluid and the solid depths and the heat flux while the output is the critical temperature difference at which convection starts. The only force that commences the evaporation is the temperature difference. It should be noted that the pressure of the vapor at the upper plate can be manipulated and reinforce the system to evaporate in the absence of temperature difference. However, the change in the pressure at the upper plate is not considered in this study. The system is analyzed by determining these input variables.

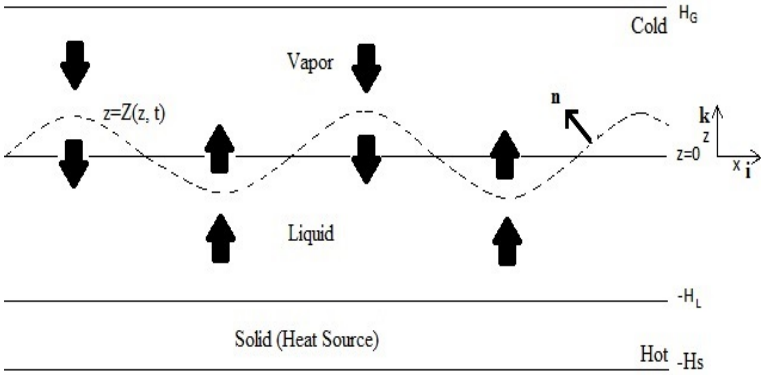

Figure 1.1. Sketch of the physical system.

Boundary conditions are another point of interest in evaporative instability. Especially, it is important to savvy how the interface temperature conditions are introduced to the system. In general, the continuity of temperature is assumed together with thermodynamic equilibrium condition. Shankar and Deshpande [11] found that the condition for temperature continuity is not valid for polyatomic components as they engender contamination at the interface and leads to temperature jump. Additionally, appliance of high temperature into the system causes the temperature jump at the interface. They claimed that the continuum calculations of Plesset [12] is wrong forasmuch as temperature jump was not considered in this study. The non-equilibrium effects on interfacial Bénard-Marangoni instability which is a free surface configuration of Rayleigh-Bénard were studied by Margerit *et al.* [13]. On the other hand, Ward and Stanga [14] came by with the continuity of the temperature at the interface as Shankar and Deshpande [11]. They elucidated that the temperature discontinuity augments

with the evaporation flux. As a result, thermodynamic equilibrium stems from low evaporation rate. In addition, lateral side walls were taken into consideration by Guo and Narayanan [15]. They studied the linear and nonlinear analysis on evaporative instability by taking the system open and closed. The closed system obviates the liquid flow much more than the vapor flow.

Mechanical perturbation prompts local evaporation and local condensation at the liquid-vapor interface for both systems, i.e. Figure 1.2 and Figure 1.3. Perturbed interface and temperature profiles are presented as dotted wave and dotted lines in both figures, respectively. The straight line at the liquid-vapor interface indicates the interface temperature profile at the base state.

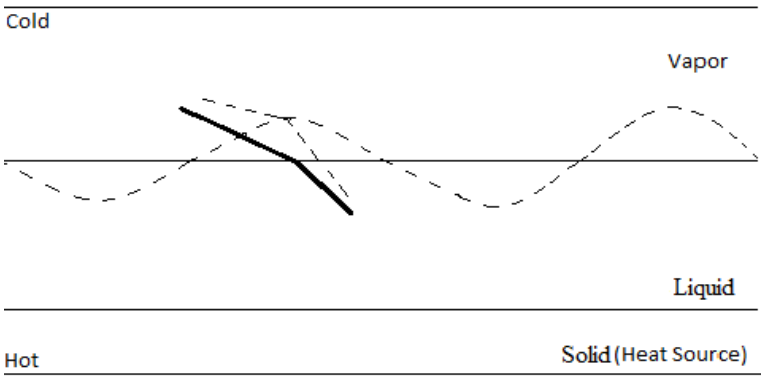

Figure 1.2. Heat input from the liquid side.

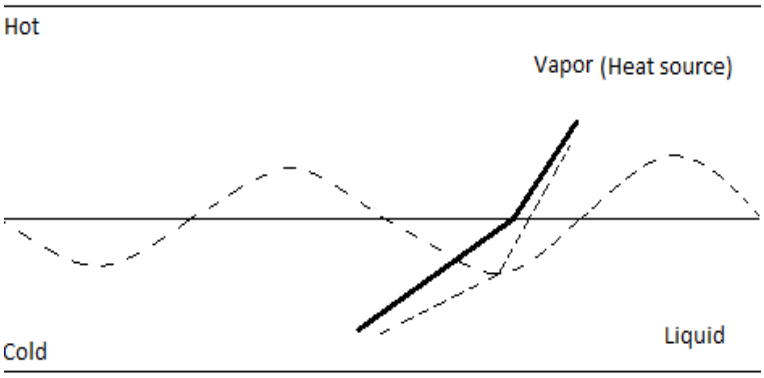

Figure 1.3. Heat input from the vapor side.

If the heat source is in the liquid side, a crest approaches to the heat sink and is far away from the heat source. Consequently, the temperature gradient is smaller

on the vapor side; therefore evaporation rate decreases on the crest which results in the unstable interface. Another way to look at the same figure is by the trough. Evaporation rate increases at the trough which now becomes closer to the hot plate; that enhances the instability. On the contrary, if the heat source is in the vapor side, this time the trough is close to the heat sink and is distant from the heat source. Similarly, one may also draw a conclusion on the stabilizing effect of evaporation by considering the crest which approaches to the heat source where the evaporation rate enhances thus flattens the interface. Additionally, these figures denote that if the interface is stable, it is stable for disturbances of all wave numbers or the other way around if the interface is unstable, it is unstable for all disturbances.

If the fluid dynamics was reckoned without any other convective effects, the temperature at the perturbed state would be the same as the temperature at the base state. In the case of heat given from the liquid side, the temperature is higher at a trough than a crest. Hence, the temperature is above the boiling point, evaporation occurs at the trough while condensation takes place at the crest where the temperature is colder than the boiling point. Since the evaporation and condensation take place locally, upward flow from the troughs and downward flow from the crests arise. Once again, instability is descried at every wave number.

Instability on the account of pressure differences are stabilized by the surface tension in fluid dynamics problems. The surface tension manifests its effect mainly at weak wave numbers. Nevertheless, the sophistication comes from the dependency of the surface tension to the temperature. Furthermore, gravity causes another complication. In the matter of light fluid at the bottom of a heavy fluid, the gravity may destabilize the system if gravitational potential energy vanquishes the surface potential energy.

In this study, merely, the instability due to pure evaporation is considered. The other effects such as temperature dependent surface tension and gravity are not taken into consideration. In addition to all of these effects, the instability can occur even in the flat interface due to the fluid motion but general case of deflecting interface is considered.

2. MATHEMATICAL MODELLING

In the mathematical modeling part, initially, all governing equations which are the momentum equations, the incompressibility conditions and the energy equations are presented. Then, the boundary conditions and the interfacial equations are introduced. All the equations are linearized and the base state and the perturbed state equations are derived. Finally, the perturbed equations are expanded into the normal mode.

The base state of the system is merely a conductive state with a flat interface. The linear stability of this base state subject to a temperature difference is investigated. At that temperature difference, named the critical temperature difference, convection starts.

2.1. Governing Equations

The Navier Stokes equations for incompressible and constant viscosity fluids are given by,

$$\rho_L \left(\frac{\partial \mathbf{v}_L}{\partial t} + \mathbf{v}_L \cdot \nabla \mathbf{v}_L \right) = -\nabla p_L + \mu_L \nabla^2 \mathbf{v}_L \tag{2.1}$$

and

$$\rho_G \left(\frac{\partial \mathbf{v}_G}{\partial t} + \mathbf{v}_G \cdot \nabla \mathbf{v}_G \right) = -\nabla p_G + \mu_G \nabla^2 \mathbf{v}_G \tag{2.2}$$

Incompressibility conditions are given as,

$$\nabla \cdot \mathbf{v}_L = 0 \tag{2.3}$$

and

$$\nabla \cdot \mathbf{v}_G = 0 \tag{2.4}$$

The problem is concerned with the temperature gradient which affects the energy transport; thus, the energy equations are required in each phase. They are presented as,

$$\frac{\partial T_S}{\partial t} = \kappa_S \nabla^2 T_S + \frac{\hat{Q}_S}{\hat{C}_{P_S}} \tag{2.5}$$

$$\frac{\partial T_L}{\partial t} + \mathbf{v}_L \cdot \nabla T_L = \kappa_L \nabla^2 T_L \tag{2.6}$$

and

$$\frac{\partial T_G}{\partial t} + \mathbf{v}_G \cdot \nabla T_G = \kappa_G \nabla^2 T_G \tag{2.7}$$

In the aforementioned equations, $\mathbf{v}$, p and T are the velocity, pressure and temperature fields, and subscripts S, L and G indicate the solid, liquid and vapor phases respectively. The parameters, $\hat{C}_P$, $\hat{Q}_S$, g, ρ, μ and κ which denote specific heat capacity at constant pressure, mass rate of thermal energy production, gravity, density, viscosity and thermal diffusivity, are assumed to be constants.

The above governing equations are solved subject to the following boundary and initial conditions, at $z = -H_S$, the bottom temperature is,

$$T_S = T_{hot} \tag{2.8}$$

At $z = -H_L$, the solid phase is considered impermeable and the condition is presented

as,

$$\mathbf{v}_L \cdot \mathbf{n} = 0 \tag{2.9}$$

where, $\mathbf{n}$ is the unit outward normal and is given by,

$$\mathbf{n} = \frac{-\frac{\partial Z}{\partial x}\mathbf{i} + \mathbf{k}}{\left(1 + \left(\frac{\partial Z}{\partial x}\right)^2\right)^{\frac{1}{2}}} \tag{2.10}$$

The derivation of the unit outward normal is given in Appendix A and $\mathbf{i}$ and $\mathbf{k}$ are the unit vectors in x and z directions. The no-slip condition is used at the solid-liquid interface as,

$$\mathbf{v}_L \cdot \mathbf{t} = 0 \tag{2.11}$$

where $\mathbf{t}$ is the unit tangent vector and presented as,

$$\mathbf{t} = \frac{\mathbf{i} + \frac{\partial Z}{\partial x}\mathbf{k}}{\left(1 + \left(\frac{\partial Z}{\partial x}\right)^2\right)^{\frac{1}{2}}} \tag{2.12}$$

The derivation of the unit tangent vector is given in Appendix A. The continuity of the temperature is given as,

$$T_S = T_L \tag{2.13}$$

Assuming Fourier's law for heat conduction, the conduction at the solid-liquid interface is equal for both phases and the condition is given by,

$$k_S \frac{\partial T_S}{\partial z} = k_L \frac{\partial T_L}{\partial z} \tag{2.14}$$

here, k denotes the thermal conductivity. At $z = H_G$, the top wall is considered

impermeable, i.e,

$$\mathbf{v}_G \cdot \mathbf{n} = 0 \tag{2.15}$$

The no-slip condition is:

$$\mathbf{v}_G \cdot \mathbf{t} = 0 \tag{2.16}$$

The top temperature is held constant as,

$$T_G = T_{cold} \tag{2.17}$$

At the liquid-vapor interface, $z = Z(t, x)$, the no-slip condition at the interface is given as,

$$\mathbf{v}_L \cdot \mathbf{t} = \mathbf{v}_G \mathbf{t} \tag{2.18}$$

The continuity of the temperature at the interface is read as,

$$T_L = T_G \tag{2.19}$$

The mass balance at the interface is read as,

$$\rho_L \left(\mathbf{v}_L - \mathbf{u}\right) \cdot \mathbf{n} = \rho_G (\mathbf{v}_G - \mathbf{u}) \cdot \mathbf{n} \tag{2.20}$$

Here, $\mathbf{u} \cdot \mathbf{n}$ is the interface speed and is given by,

$$\mathbf{u} \cdot \mathbf{n} = \frac{\frac{\partial Z}{\partial t}}{\left(1 + \left(\frac{\partial Z}{\partial x}\right)^2\right)^{1/2}} \tag{2.21}$$

The derivation of the interface speed is given in Appendix A. The total stress balance

at the interface is read as,

$$\{\rho_L (\mathbf{v}_L - \mathbf{u}) \mathbf{v}_L - \boldsymbol{T}_L\} \cdot \mathbf{n} + \gamma 2H\mathbf{n} = \{\rho_G (\mathbf{v}_G - \mathbf{u}) \mathbf{v}_G - \boldsymbol{T}_G\} \cdot \mathbf{n} \tag{2.22}$$

Equation 2.22 is rearranged by using Eq. 2.20 and is presented as,

$$\{\rho_L (\mathbf{v}_L - \mathbf{u}) (\mathbf{v}_L - \mathbf{v_G}) - (\boldsymbol{T}_L - \boldsymbol{T}_G)\} \cdot \mathbf{n} + \gamma 2H\mathbf{n} = \mathbf{0} \tag{2.23}$$

Here, $\boldsymbol{T}$, γ and $2H$ are the total stress tensor, the interfacial tension, and twice of the surface mean curvature. The total stress tensor,$\boldsymbol{T}$ and twice the surface mean curvature, $2H$, are given as,

$$\boldsymbol{T} = -p\mathbf{I} + \boldsymbol{S} \tag{2.24}$$

and

$$2H = \frac{\frac{\partial^2 Z}{\partial x^2}}{\left(1 + \left(\frac{\partial Z}{\partial x}\right)^2\right)^{3/2}} \tag{2.25}$$

The total stress tensor is inserted into Eq. 2.23 and is read as,

$$\{\rho_L (\mathbf{v}_L - \mathbf{u}) (\mathbf{v}_L - \mathbf{v_G}) - [(p_G - p_L) \mathbf{I} + (\boldsymbol{S}_L - \boldsymbol{S}_G)]\} \cdot \mathbf{n} + \gamma 2H\mathbf{n} = \mathbf{0} \tag{2.26}$$

where $\mathbf{I}$ is the identity tensor and $\boldsymbol{S}$ is the deviatoric part of the stress tensor. Additionally, the energy balance is required, which is given as,

$$\rho_L (\mathbf{v}_L - \mathbf{u}) \left\{ \left(\hat{U}_L - \hat{U}_G\right) + \frac{1}{2} \left(|\mathbf{v}_L|^2 - |\mathbf{v}_G|^2\right) \right\} \cdot \mathbf{n} + (\mathbf{q}_L - \mathbf{q}_G) \cdot \mathbf{n} - \{\boldsymbol{T}_L \cdot \mathbf{v}_L - \boldsymbol{T}_G \cdot \mathbf{v}_G\} \cdot \mathbf{n} + \gamma 2H\mathbf{n} \cdot \mathbf{u} = 0 \tag{2.27}$$

where, $\hat{U}$ stands for internal energy per unit mass and note that Eq. 2.27 is frame-variant and it is subjected to an algebraic manipulation that is given in details in

Appendix B to make the equation frame-invariant as,

$$\rho_L \left(\mathbf{v}_L - \mathbf{u}\right) \left\{ \left(\hat{H}_L - \hat{H}_G\right) + \frac{1}{2}\left(\left(\mathbf{v}_L - \mathbf{u}\right)^2 - \left(\mathbf{v}_G - \mathbf{u}\right)^2\right) \right\} \cdot \mathbf{n} + \left(\mathbf{q}_L - \mathbf{q}_G\right) \cdot \mathbf{n} - \left\{ \boldsymbol{S}_L \cdot \left(\mathbf{v}_L - \mathbf{u}\right) - \boldsymbol{S}_G \cdot \left(\mathbf{v}_G - \mathbf{u}\right) \right\} \cdot \mathbf{n} = \mathbf{0} \quad (2.28)$$

where $\hat{H}$ and $\mathbf{q}$ are the enthalpy per unit mass and the heat flux vector, respectively and the heat flux is given by Fourier's law as,

$$\mathbf{q} = -k \nabla T \quad (2.29)$$

Eq. 2.28 is rearranged by using the heat flux definition as,

$$\rho_L \left(\mathbf{v}_L - \mathbf{u}\right) \left\{ \left(\hat{H}_L - \hat{H}_G\right) + \frac{1}{2}\left(\left(\mathbf{v}_L - \mathbf{u}\right)^2 - \left(\mathbf{v}_G - \mathbf{u}\right)^2\right) \right\} \cdot \mathbf{n} - \left(k_L \nabla T_L - k_G \nabla T_G\right) \cdot \mathbf{n} - \left\{ \boldsymbol{S}_L \cdot \left(\mathbf{v}_L - \mathbf{u}\right) - \boldsymbol{S}_G \cdot \left(\mathbf{v}_G - \mathbf{u}\right) \right\} \cdot \mathbf{n} = \mathbf{0} \quad (2.30)$$

To close the problem, the Clausius Clapeyron equation is used as an equilibrium relationship and given by,

$$\left(P_G - P_{G_0}\right) - \rho_G \, \mathcal{L} \, ln \left(\frac{T_G}{T_{G_0}}\right) = 0 \quad (2.31)$$

Here, P_{G_0} and $T_{G_0}$are the base state temperatures of the fluid and $\mathcal{L}$ is the latent heat of evaporation which is given by,

$$\mathcal{L} = \hat{H}_L - \hat{H}_G \quad (2.32)$$

2.2. Scaled Governing Equations

The governing equations are presented in their dimensionless form by using the following scales,

Liquid depth $(-H_L)$	$:H_L$
Velocity	$:\frac{\kappa_L}{H_L}$
Time	$:\frac{H_L}{\bar{v}}$, $\frac{H_L^2}{\kappa_L}$
Pressure	$:\frac{\mu_L \bar{v}}{H_L}$, $\frac{\mu_L \kappa_L}{H_L^2}$
Temperature	$: \frac{T-T_{cold}}{\triangle T}$
Heat	$: \frac{k_L \triangle T}{H_L}$

Velocity scaling is performed by considering the thermal diffusivity that serves for the dissipation of the temperature perturbations because the temperature gradient leads to an instability in this problem. Heat flux is scaled by assuming Fourier's law for the heat conduction. The temperature difference, $\triangle T$, is taken as $(T_{hot} - T_{cold})$ where T_{cold} is the reference temperature. Recall that in the study, the top, T_{cold}, and the bottom, T_{hot}, temperatures are kept constant. The dimensionless form is denoted by asterisk.

The dimensionless momentum equations are read respectively for the liquid and the vapor phases as,

$$\frac{1}{Pr}\left(\frac{\partial \mathbf{v}_L^*}{\partial t^*} + \mathbf{v}_L^* \cdot \nabla \mathbf{v}_L^*\right) = -\nabla p_L^* + \nabla^2 \mathbf{v}_L^* \tag{2.33}$$

and

$$\frac{1}{Pr}\frac{\nu_L}{\nu_G}\left(\frac{\partial \mathbf{v}_G^*}{\partial t^*} + \mathbf{v}_G^* \cdot \nabla \mathbf{v}_G^*\right) = -\frac{\mu_L}{\mu_G}\nabla p_G^* + \nabla^2 \mathbf{v}_G^* \tag{2.34}$$

Here,

$$Pr = \frac{\nu_L}{\kappa_L} \tag{2.35}$$

where Pr is the Prandtl number.

The scaled incompressibility conditions are,

$$\nabla \cdot \mathbf{v}_L^* = 0 \tag{2.36}$$

for the liquid phase and

$$\nabla \cdot \mathbf{v}_G^* = 0 \tag{2.37}$$

for the vapor phase.

The dimensionless energy equations are,

$$\frac{\kappa_L}{\kappa_S}\frac{\partial T_S^*}{\partial t^*} = \nabla^2 T_S^* + \phi \tag{2.38}$$

where,

$$\phi = \frac{H_L^2 \hat{Q}_S}{\triangle T\, \hat{C}_{P_S} \kappa_S} \tag{2.39}$$

$$\frac{\partial T_L^*}{\partial t^*} + (\boldsymbol{v}_L^* \cdot \nabla T_L^*) = \nabla^2 T_L^* \tag{2.40}$$

and

$$\frac{\kappa_L}{\kappa_G}\left(\frac{\partial T_G^*}{\partial t^*} + (\boldsymbol{v}_G^* \cdot \nabla T_G^*)\right) = \nabla^2 T_G^* \tag{2.41}$$

2.3. Scaled Boundary and Interface Conditions

The scaled boundary conditions are presented as, at $z^* = -H_S^*$. The scaled bottom temperature is,

$$T_S^* = 1 \tag{2.42}$$

At the solid-liquid interface, located at $z^* = -1$, the scaled impermeable condition is,

$$\mathbf{v}_L^* \cdot \mathbf{n} = 0 \tag{2.43}$$

The scaled no-slip condition is,

$$\mathbf{v}_L^* \cdot \mathbf{t} = 0 \tag{2.44}$$

The scaled continuity of the temperature is given as,

$$T_S^* = T_L^* \tag{2.45}$$

Assuming Fourier's law for heat conduction, the conduction at the solid-liquid interface is equal for both phases and the condition is given by,

$$\frac{\partial T_S^*}{\partial z^*} = \frac{k_L}{k_S}\frac{\partial T_L^*}{\partial z^*} \tag{2.46}$$

At $z^* = H_G^*$, the scaled impermeable top wall condition is,

$$\mathbf{v}_G^* \cdot \mathbf{n} = 0 \tag{2.47}$$

The scaled no-slip condition is,

$$\mathbf{v}_G^* \cdot \mathbf{t} = 0 \tag{2.48}$$

The scaled top temperature is,

$$T_G^* = 0 \tag{2.49}$$

At the liquid-vapor interface, $z^* = Z^*(t,x)$, the no slip condition at the interface is given as,

$$\mathbf{v}_L^* \cdot \mathbf{t} = \mathbf{v}_G^* \cdot \mathbf{t} \tag{2.50}$$

The continuity of the temperature at the interface is read as,

$$T_L^* = T_G^* \tag{2.51}$$

The dimensionless mass conservation equation at the interface is presented as,

$$(\mathbf{v}_L^* - \mathbf{u}^*) \cdot \mathbf{n} - \frac{\rho_G}{\rho_L}(\mathbf{v}_G^* - \mathbf{u}^*) \cdot \mathbf{n} = 0 \tag{2.52}$$

The dimensionless stress balance equation at the interface, $z^* = Z^*(x,t)$, is presented as,

$$Ca\left\{\frac{1}{Pr}\left(\mathbf{v}_L^* - \mathbf{u}^*\right)\left(\mathbf{v}_L^* - \mathbf{v}_G^*\right) - \left(\left[\left(p_G^* - p_L^*\right)\mathbf{I} + \left(\boldsymbol{S}_L^* - \frac{\mu_G}{\mu_L}\boldsymbol{S}_G^*\right)\right]\right)\right\} \cdot \mathbf{n} + 2H^*\mathbf{n} = \mathbf{0} \tag{2.53}$$

Here,

$$Ca = \frac{\mu_L \kappa_L}{\gamma H_L}$$

where Ca is the thermal capillary number. The capillary number indicates the ratio of the viscous to surface tension forces, The normal component of the stress balance is presented as,

$$Ca\left\{\left(p_L^* - p_G^*\right) - 2\left(\frac{\partial v_{L_Z}^*}{\partial z^*} - \frac{\mu_G}{\mu_L}\frac{\partial v_{G_Z}^*}{\partial z^*}\right)\right\} + 2H^* = 0 \tag{2.54}$$

The tangential component of the stress balance is read as,

$$\left(\frac{\partial v_{L_X}^*}{\partial z^*} + \frac{\partial v_{L_Z}^*}{\partial x^*}\right) - \frac{\mu_G}{\mu_L}\left(\frac{\partial v_{G_X}^*}{\partial z^*} + \frac{\partial v_{G_Z}^*}{\partial x^*}\right) = 0 \tag{2.55}$$

The dimensionless energy conservation equation at the interface is derived as,

$$\begin{aligned}&(\mathbf{v}_L^* - \mathbf{u}^*)\left\{1 + \frac{1}{2}K\left((\mathbf{v}_L^* - \mathbf{u}^*)^2 - (\mathbf{v}_G^* - \mathbf{u}^*)^2\right)\right\}\cdot\mathbf{n}\\ &- E\left(\nabla T_L^* - \frac{k_G}{k_L}\nabla T_G^*\right)\cdot\mathbf{n} - V\left\{\boldsymbol{S}_L^*\cdot(\mathbf{v}_L^* - \mathbf{u}^*) - \frac{\mu_G}{\mu_L}\boldsymbol{S}_G^*\cdot(\mathbf{v}_G^* - \mathbf{u}^*)\right\}\mathbf{n} = 0\end{aligned} \tag{2.56}$$

Here,

$$K = \frac{\kappa_L^2}{\mathcal{L}H_L^2} \tag{2.57}$$

$$V = \frac{\nu_L\kappa_L}{\mathcal{L}H_L^2} \tag{2.58}$$

$$E = \frac{k_L\triangle T}{\kappa_L\rho_L\mathcal{L}} \tag{2.59}$$

Here, E is the evaporation number. The scaled Clausius Clapeyron equation is,

$$\Pi_{KE}\left(P_G^* - P_{G_0}^*\right) - ln\left(\frac{T_G^*}{T_{G_0}^*}\right) = 0 \tag{2.60}$$

where,

$$\Pi_{KE} = \frac{\rho_L}{\rho_G}\frac{\nu_L\kappa_L}{\mathcal{L}H_L^2} \tag{2.61}$$

2.4. Scaled Base State

The problem is linearized about a base state which is the flat interface for this problem to obtain the commencement of the interfacial instability that comes from the perturbed model. The base state is stationary; therefore there is no need to have mass and momentum equations for velocity. Merely, the momentum equations are used to find the pressure profiles. In addition, the base state is a steady conducting phase in the z direction.

2.4.1. Domain Equations and Boundary Conditions

The scaled momentum equations for the liquid and the vapor phases at the base state are read as,

$$-\nabla_0^* p_{L_0}^* = 0 \tag{2.62}$$

$$-\frac{\rho_L}{\rho_G}\nabla_0^* p_{G_0}^* = 0 \tag{2.63}$$

The scaled energy equation for the solid phase at the base state is,

$$\nabla_0^2 T_{S_0}^* + \phi = 0 \tag{2.64}$$

$$\nabla_0^2 T_{L_0}^* = 0 \tag{2.65}$$

for the liquid phase and

$$\nabla_0^2 T_{G_0}^* = 0 \tag{2.66}$$

for the vapor phase.

The boundary conditions at the base state are presented as, at $z^* = -H_S^*$, the scaled bottom temperature is,

$$T_{S_0}^* = 1 \tag{2.67}$$

At $z^* = -H_L^*$, the scaled continuity of temperature at the base state is given as,

$$T_{S_0}^* = T_{L_0}^* \tag{2.68}$$

The scaled equal heat fluxes at the base state are presented as,

$$\frac{dT_{S_0}^*}{dz_0^*} = \frac{k_L}{k_S}\frac{dT_{L_0}^*}{dz_0^*} \tag{2.69}$$

At $z^* = 0$, the scaled continuity of the temperature at the interface is read as,

$$T_{L_0}^* = T_{G_0}^* \tag{2.70}$$

The scaled heat fluxes at the base state are read as,

$$\frac{dT_{L_0}^*}{dz_0^*} = \frac{k_G}{k_L}\frac{dT_{G_0}^*}{dz_0^*} \tag{2.71}$$

At $z^* = H_G^*$, the scaled top temperature at the base state is held constant as,

$$T_{G_0}^* = 0 \tag{2.72}$$

2.5. Base Sate Solution

The base state solution for the temperature profiles are,

$$T_{S_0}^*(z) = -\phi\frac{z^{*^2}}{2} + C_1 z^* + C_2 \tag{2.73}$$

for the solid,

$$T^*_{L_0} = C_3 z^* + C_4 \tag{2.74}$$

for the liquid phase and,

$$T^*_{G_0} = C_5 z^* + C_6 \tag{2.75}$$

for the vapor phase. Here,

$$C_1 = \frac{\frac{\phi}{2}\left\{\left[1 - 2\left(\frac{k_S}{k_L} - \frac{k_S H_G}{k_G H_L}\right)\right] H_L^2 - H_S^2\right\}}{H_S + \left(\frac{k_S}{k_L} - 1\right) H_L + \frac{k_S}{k_G} H_G} \tag{2.76}$$

$$C_2 = 1 + \phi\frac{H_S^2}{2} + C_1 H_S \tag{2.77}$$

$$C_3 = \frac{k_S}{k_L}\left(\phi H_L + C_1\right) \tag{2.78}$$

$$C_4 = \frac{\phi}{2}\left\{H_S^2 - \left(1 - \frac{k_S}{k_L}\right) H_L^2\right\} + \left\{H_S - \left(1 - \frac{k_S}{k_L}\right) H_L C_1\right\} + 1 \tag{2.79}$$

$$C_5 = \frac{k_S}{k_G}\left(\phi H_L + C_1\right) \tag{2.80}$$

and

$$C_6 = -\frac{k_S}{k_G} H_G \left(\phi H_L + C_1\right) \tag{2.81}$$

The base state solution for the pressure gradients in the liquid and the vapor phases are presented as,

$$\frac{dp^*_{L_0}}{dz^*_0} = 0 \tag{2.82}$$

and

$$\frac{dp^*_{G_0}}{dz^*_0} = 0 \tag{2.83}$$

respectively.

2.6. Scaled Perturbed State

The scaled momentum equations for the liquid and the vapor phases at the perturbed state are read as,

$$\frac{1}{Pr}\frac{\partial \mathbf{v}^*_{L_1}}{\partial t^*_0} = -\nabla_0 p^*_{L_1} + \nabla^2_0 \mathbf{v}^*_{L_1} \tag{2.84}$$

and

$$\frac{1}{Pr}\frac{\nu_L}{\nu_G}\frac{\partial \mathbf{v}^*_{G_1}}{\partial t^*_0} = -\frac{\mu_L}{\mu_G}\nabla_0 p^*_{G_1} + \nabla^2_0 \mathbf{v}^*_{G_1} \tag{2.85}$$

The scaled energy equations for the solid, the liquid and the vapor at the perturbed state are presented as,

$$\frac{\kappa_L}{\kappa_S}\frac{\partial T^*_{S_1}}{\partial t^*_0} = \nabla^{2^*}_0 T^*_{S_1} \tag{2.86}$$

$$\frac{\partial T^*_{L_1}}{\partial t^*_0} + \frac{\partial T^*_{L_0}}{\partial z^*_0} v^*_{L_{Z_1}} = \nabla^{2^*}_0 T^*_{L_1} \tag{2.87}$$

and

$$\frac{\kappa_L}{\kappa_G}\frac{\partial T^*_{G_1}}{\partial t^*_0} + \frac{\kappa_L}{\kappa_G}\frac{\partial T^*_{G_0}}{\partial z^*_0} v^*_{G_{Z_1}} = \nabla^{2^*}_0 T^*_{G_1} \tag{2.88}$$

respectively.

The scaled boundary conditions at perturbed state are presented as, at $z^* = -H^*_S$: The scaled bottom temperature is,

$$T^*_{S_1} = 0 \tag{2.89}$$

At $z^* = -1$, the scaled impermeable condition is,

$$\mathbf{v}^*_{L_{Z_1}} = 0 \tag{2.90}$$

The scaled no-slip condition is,

$$\mathbf{v}^*_{L_{X_1}} = 0 \tag{2.91}$$

Assuming Fourier's law for heat conduction, the conduction at the solid-liquid interface is equal for both phases and the condition is given by,

$$\frac{\partial T^*_{S_1}}{\partial z^*_0} = \frac{k_L}{k_S}\frac{\partial T^*_{L_1}}{\partial z^*_0} \tag{2.92}$$

At $z^* = H^*_G$, the scaled impermeable top wall condition is,

$$\mathbf{v}^*_{G_{Z_1}} = 0 \tag{2.93}$$

The scaled no-slip condition is,

$$\mathbf{v}^*_{G_{X_1}} = 0 \tag{2.94}$$

The scaled top temperature is,

$$T^*_{G_1} = 0 \tag{2.95}$$

At the liquid-vapor interface, $z^* = 0$, the no slip condition at the interface is given as,

$$\mathbf{v}^*_{L_{X_1}} = \mathbf{v}^*_{G_{X_1}} \tag{2.96}$$

The continuity of the temperature at the interface is read as,

$$T^*_{L_1} + \frac{dT^*_{L_0}}{dz^*_0} Z^*_1 = T^*_{G_1} + \frac{dT^*_{G_0}}{dz^*_0} Z^*_1 \tag{2.97}$$

The unit normal vector to order ε is presented as,

$$\mathbf{n} = \mathbf{n_0} + \varepsilon \mathbf{n_1} \tag{2.98}$$

where,

$$\mathbf{n_0} = \mathbf{k} \tag{2.99}$$

and

$$\mathbf{n_1} = -\frac{\partial Z_1}{\partial x_0}\mathbf{i} \tag{2.100}$$

The mass balance at the interface for the perturbed state is,

$$\left(v^*_{L_{Z_1}} - \frac{\partial Z^*_1}{\partial t^*_0}\right) = \frac{\rho_G}{\rho_L}\left(v^*_{G_{Z_1}} - \frac{\partial Z^*_1}{\partial t^*_\mathbf{0}}\right) \tag{2.101}$$

The twice of the scaled mean surface curvature in the normal component of the stress

balance equation at the perturbed state is given as,

$$2H_1^* = \frac{\partial^2 Z_1^*}{\partial x_0^{2^*}} \tag{2.102}$$

The scaled normal component of the stress balance at the perturbed state is presented as,

$$Ca\left\{\left(p_{L_1}^* - p_{G_1}^*\right) + Z_1\left(\frac{dp_{L_0}^*}{dz_0^*} - \frac{dp_{G_0}^*}{dz_0^*}\right) - 2\left(\frac{\partial v_{L_{Z_1}}^*}{\partial z_0^*} - \frac{\mu_G}{\mu_L}\frac{\partial v_{G_{Z_1}}^*}{\partial z_0^*}\right)\right\} + \frac{\partial^2 Z_1^*}{\partial x_0^{2^*}} = 0 \tag{2.103}$$

The scaled tangential component of the stress balance at the perturbed state is given as,

$$\left(\frac{\partial v_{L_{X_1}}^*}{\partial z_0^*} + \frac{\partial v_{L_{Z_1}}^*}{\partial x_0^*}\right) - \frac{\mu_G}{\mu_L}\left(\frac{\partial v_{G_{X_1}}^*}{\partial z_0^*} + \frac{\partial v_{G_{Z_1}}^*}{\partial x_0^*}\right) = 0 \tag{2.104}$$

The scaled energy conservation equation at the perturbed state is read as,

$$E\left\{\left(\frac{\partial T_{L_1}^*}{\partial z_0^*} + Z_1^*\frac{\partial^2 T_{L_0}^*}{\partial z_0^{2^*}}\right) - \frac{k_G}{k_L}\left(\frac{\partial T_{G_1}^*}{\partial z_0^*} + Z_1^*\frac{\partial^2 T_{G_0}^*}{\partial z_0^{2^*}}\right)\right\} + \left(v_{L_{Z_1}}^* - \frac{\partial Z_1^*}{\partial t^*}\right) = 0 \tag{2.105}$$

The scaled Clausius Clapeyron equation at the perturbed state is,

$$\Pi_{KE}\left(P_{G_1}^* + \frac{dp_0^*}{dz_0^*}Z_1^*\right) - \frac{1}{T_{G_0}^*}\left(T_{G_1}^* + \frac{dT_{G_0}^*}{dz_0^*}Z_1^*\right) = 0 \tag{2.106}$$

2.7. Normal Mode Expansion

The set of partial differential equations are turned into an eigenvalue problem by using the normal mode expansion [16] which is shown on the liquid velocity as,

$$\mathbf{v}_{L_1}^*(x,z,t) = \tilde{\mathbf{v}}_{L_1}(z)e^{\sigma t}e^{ikx} + \bar{\tilde{\mathbf{v}}}_{L_1}(z)e^{\sigma t}e^{-ikx} \tag{2.107}$$

where k is the wave number and σ is the growth constant of the given disturbance. Also the over bar in $\bar{\tilde{\mathbf{v}}}_{L_1}$represents the complex conjugate.

2.7.1. Scaled Perturbed Equations After Normal Mode Expansion

The momentum equations in the x and z directions for the liquid and vapor phases are presented as,

$$\frac{1}{Pr}\sigma\tilde{v}_{L_{X_1}} = -ik\tilde{p}_{L_1} + \left(\frac{d^2}{dz_0^2} - k^2\right)\tilde{v}_{L_{X_1}} \tag{2.108}$$

$$\frac{1}{Pr}\sigma\tilde{v}_{L_{Z_1}} = -\frac{d\tilde{p}_{L_1}}{dz_0} + \left(\frac{d^2}{dz_0^2} - k^2\right)\tilde{v}_{L_{Z_1}} \tag{2.109}$$

$$\frac{1}{Pr}\frac{\nu_L}{\nu_G}\sigma\tilde{v}_{G_{X_1}} = -\frac{\mu_L}{\mu_G}ik\tilde{p}_{G_1} + \left(\frac{d^2}{dz_0^2} - k^2\right)\tilde{v}_{G_{X_1}} \tag{2.110}$$

and

$$\frac{1}{Pr}\frac{\nu_L}{\nu_G}\sigma\tilde{v}_{G_{Z_1}} = -\frac{\mu_L}{\mu_G}\frac{d\tilde{p}_{G_1}}{dz_0} + \left(\frac{d^2}{dz_0^{*2}} - k^2\right)\tilde{v}_{G_{Z_1}} \tag{2.111}$$

respectively.

Continuity equations are read for the liquid and the vapor as,

$$ik\tilde{v}_{L_{X_1}} + \frac{d\tilde{v}_{L_{Z_1}}}{dz_0} = 0 \tag{2.112}$$

and

$$ik\tilde{v}_{G_{X_1}} + \frac{d\tilde{v}_{G_{Z_1}}}{dz_0} = 0 \tag{2.113}$$

The energy equations are presented for the solid, the liquid and the

$$\sigma \frac{\kappa_L}{\kappa_S} \tilde{T}_{S_1} = \left(\frac{d^2}{dz_0^2} - k^2 \right) \tilde{T}_{S_1} \tag{2.114}$$

$$\sigma \tilde{T}_{L_1} + \frac{dT_{L_0}}{dz_0} \tilde{v}_{L_{Z_1}} = \left(\frac{d^2}{dz_0^2} - k^2 \right) \tilde{T}_{L_1} \tag{2.115}$$

$$\sigma \frac{\kappa_L}{\kappa_G} \tilde{T}_{G_1} + \frac{\kappa_L}{\kappa_G} \frac{\partial dT_{G_0}}{dz_0} \tilde{v}_{G_{Z_1}} = \left(\frac{d^2}{dz_0^2} - k^2 \right) \tilde{T}_{G_1} \tag{2.116}$$

The scaled boundary conditions at the perturbed state are subject to normal mode expansion as, at $z^* = -H_S^*$, the scaled bottom temperature is,

$$\tilde{T}_{S_1} = 0 \tag{2.117}$$

At $z^* = -1$, the scaled impermeable condition is,

$$\tilde{v}_{L_{Z_1}} = 0 \tag{2.118}$$

The scaled no slip condition is,

$$\tilde{v}_{L_{X_1}} = 0 \tag{2.119}$$

The continuity of the temperature at the interface is read as,

$$\tilde{T}_{S_1} = \tilde{T}_{L_1} \tag{2.120}$$

Heat fluxes for both phases are read by,

$$\frac{d\tilde{T}_{S_1}}{dz_0} = \frac{k_L}{k_S}\frac{d\tilde{T}_{L_1}}{dz_0} \tag{2.121}$$

At $z^* = H_G^*$, the scaled impermeable top wall condition is,

$$\tilde{v}_{G_{Z_1}} = 0 \tag{2.122}$$

The scaled no-slip condition is,

$$\tilde{v}_{G_{X_1}} = 0 \tag{2.123}$$

The scaled top temperature is,

$$\tilde{T}_{G_1} = 0 \tag{2.124}$$

At the liquid-vapor interface, $z^* = 0$, the no-slip condition at the interface is given as,

$$\tilde{v}_{L_{X_1}} = \tilde{v}_{G_{X_1}} \tag{2.125}$$

The continuity of the temperature at the interface is read as,

$$\tilde{T}_{L_1} + \frac{dT_{L_0}}{dz_0}\tilde{Z}_1 = \tilde{T}_{G_1} + \frac{dT_{G_0}}{dz_0}\tilde{Z}_1 \tag{2.126}$$

The scaled mass conservation equation is presented as,

$$\left(\tilde{v}_{L_{Z_1}} - \sigma\tilde{Z}_1\right) - \frac{\rho_G}{\rho_L}\left(\tilde{v}_{G_{Z_1}} - \sigma\tilde{Z}_1\right) = 0 \tag{2.127}$$

The scaled stress balance equation is presented, respectively for the normal and the

tangential components as

$$Ca\left\{(\tilde{p}_{L_1}-\tilde{p}_{G_1})+\tilde{Z}_1\left(\frac{dp_{L_0}}{dz_0}-\frac{dp_{G_0}}{dz_0}\right)-2\left[\frac{d\tilde{v}_{L_{Z_1}}}{dz_0}-\frac{\mu_G}{\mu_L}\frac{d\tilde{v}_{G_{Z_1}}}{dz_0}\right]\right\} - k^2\tilde{Z}_1 = 0 \quad (2.128)$$

and

$$\frac{d\tilde{v}_{L_{X_1}}}{dz_0}+ik\tilde{v}_{L_{Z_1}}-\frac{\mu_G}{\mu_L}\left(\frac{d\tilde{v}_{G_{X_1}}}{dz_0^*}+ik\tilde{v}_{G_{Z_1}}\right)=0 \quad (2.129)$$

The scaled energy conservation equation is,

$$E\left\{\frac{d\tilde{T}_{L_1}}{dz_0}+\tilde{Z}_1\frac{d^2T_{L_0}}{dz_0^2}-\frac{k_G}{k_L}\left(\frac{d\tilde{T}_{G_1}}{dz_0}+\tilde{Z}_1\frac{d^2T_{G_0}}{dz_0^2}\right)\right\} + \left(\tilde{v}_{L_{Z_1}}-\sigma\tilde{Z}_1\right)=0 \quad (2.130)$$

The scaled Clausius Clapeyron equation is,

$$\Pi_{KE}\left(\tilde{p}_{G_1}-\frac{dp_0}{dz_0}\tilde{Z}_1\right)-\frac{1}{T_{G_0}}\left(\tilde{T}_{G_1}+\frac{dT_{G_0}}{dz_0}\tilde{Z}_1\right)=0 \quad (2.131)$$

2.8. Solution Procedure

The solution for the linear ordinary differential equations is performed by using the Chebyshev-Spectral method [17]. The equations in the study are turned into an eigenvalue problem. The eigenvalue is either σ or the evaporation number, E, when σ is set equal to zero. The graphs of σ and evaporation number, E, versus wave number with different parameters are analyzed in the study.

3. RESULTS AND DISCUSSIONS

The linear stability of the solid-liquid-vapor system heated from the solid side is investigated. The solid part of the system is used as a heat source and the effect of this heat source on the linear stability is explained. In the system, the physical parameters are assumed to be constant. Inputs are the heat, the physical parameters, the depths of the solid, the liquid and the vapor phases while the output is the temperature difference at which convection starts. The physical properties for the liquid at 100°C and its saturated vapor under atmospheric pressure.

In the mathematical modeling part, initially, the set of partial differential equations are linearized and the problem is turned into an eigenvalue problem via the normal mode expansion. When it comes to the interface equations, all of them are rendered frame invariant. This can be observed in the force and the energy equations. The nonlinearities in the equations stem from the domain variables such as the effect of the interface temperature profile on the pressure profile that also affects the flow profiles. Finally, the problem is solved by using the Chebyshev spectral method [17].

The boundary conditions are completed by the Clausius Clapeyron equation as low evaporation rate is conjectured. Due to low evaporation rate, it could also be assumed that there is thermodynamic equilibrium at the interface. By making use of this conjecture, the Clausius Clapeyron equation could be derived. It is important to note that the equation solely comprises the perturbed pressure and temperature terms from the vapor side.

It is important to bring the dimensionless numbers to the attention. The important dimensionless numbers in this study are the evaporation number and the heat source numbers denoted as E and ϕ, respectively. Both dimensionless numbers include the temperature difference as a variable. Evaporation number which appears in the energy balance equation increases with the temperture difference. On the other hand, the heat source number has one more variable which is the heat flux. Note that again the

heat flux is taken as to be constant in this study for the sake of simplicity. Comprising the two variables means that their values would change in terms of one another at a constant value of heat source number that makes the problem interesting. The physical meaning of the evaporation and heat source numbers relies on the temperature difference that literally gives the critical temperature difference at which convection starts.

The surface tension gradient and the effect of gravity are omitted. The surface tension gradient and the effect of gravity relates to Marangoni convection and Rayleigh convection, respectively. In the absence of gravity, pressure gradient does not exist at the base state and this makes the problem easier to cope with.

3.1. Effect of Heat Source Number on the Critical Evaporation Number

The effect of small values of heat source number on the evaporation number is presented in Figure 3.1. It was found that the small values of the dimensionless heat source has no effect on the evaporation number up to a value of 0.01. After this verge, the evaporation number dwindles for large values of heat source number that is indicated in Figure 3.2 and attains a saturation point but it is not indicated in the figure. When the evaporation number decreases, the system becomes unstable as the temperature increases at the interface. Each curve represents a neutral curve, above which the system is unstable and below which it is stable to given disturbances.

The dimensionless vapor depth is taken as 0.1 to be able to make a comparison with the study of Ozen and Narayanan [18]. The result of Ozen and Narayanan [18] is recovered by taking the heat source as zero.

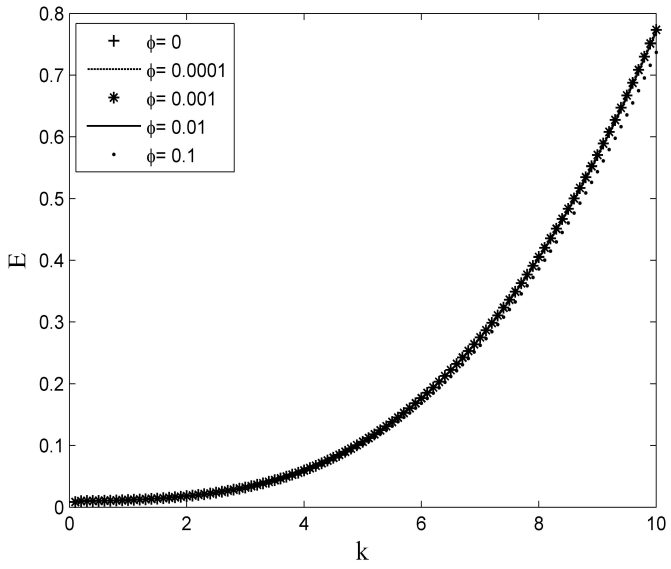

Figure 3.1. Critical evaporation number versus wave number for small values of dimensionless heat source for $H_S = 1$ and $H_G = 0.1$.

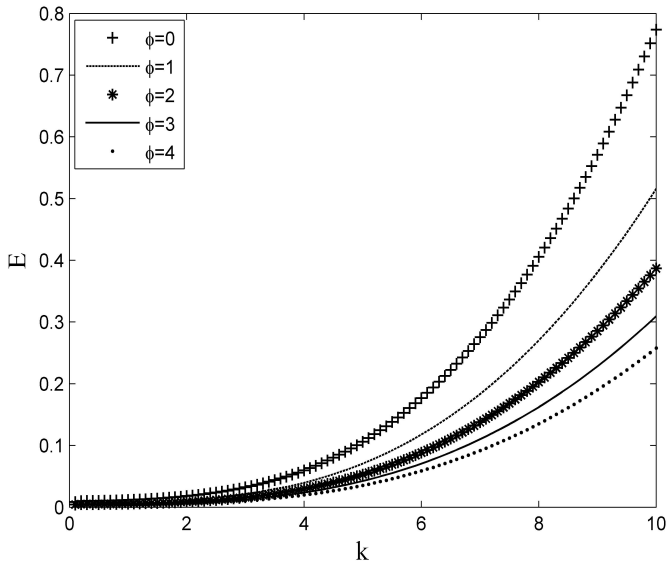

Figure 3.2. Critical evaporation number versus wave number for large values of dimensionless heat source for $H_S = 1$ and $H_G = 0.1$.

Figures 3.3 and 3.4 depict the behavior of the temperature profile at the base state. The difference between these two figures is the value of the dimensionless heat source that is 1 for Figure 3.3 and 4 for Figure 3.4. It is concluded that the the base state temperature increases with heat source number. It can be figured out from

the figures that the temperature difference between the vapor and the liquid phases increases owing to the solid phase.

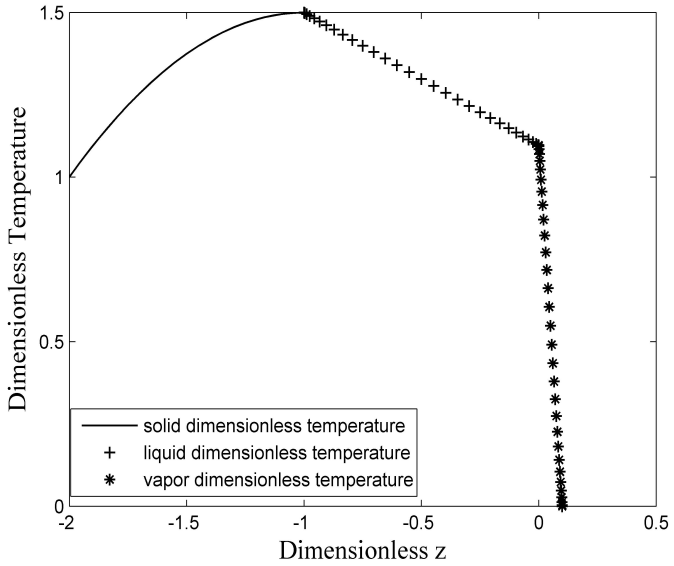

Figure 3.3. Dimensionless base temperature versus dimensionless position for $\phi = 1$, $H_S = 1$, $H_G = 0.1$.

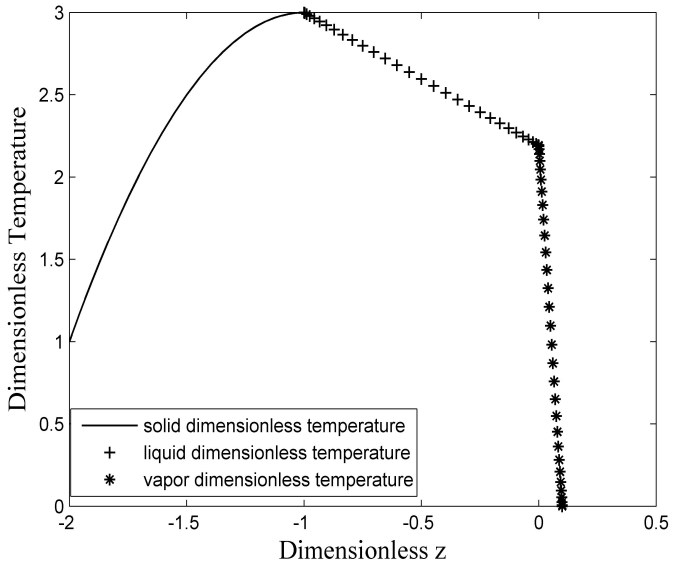

Figure 3.4. Dimensionless base temperature versus dimensionless position for $\phi = 4$, $H_S = 1$, $H_G = 0.1$.

3.2. Effect of Vapor Depth on Dispersion Curve

In the previous studies, it was found that the vapor depth increment makes the system more stable due to its thermal resistance and the vapor flow. However, after a point vapor depth does not affect the system stability because of the thermal diffusivity. In this study, again the same result is found and it is depicted in Figure Figure 3.5 for small values and 3.6 for large values of vapor depth. However, two-phase system, liquid-vapor, is more stable than the three-phase system, solid-liquid-vapor, because there is a heat source in the three phase system which increases the interface temperature between the solid and the liquid. The effect of heat source on interfacial instability can be seen in the base state solution that contains the heat source number in the solid part of the energy equation.

Figures 3.7 and 3.8 shows the dispersion curves to investigate the behavior of the system at weak wavenumbers for small and large values of vapor depth, respectively. Abrupt increment was observed at weak wave numbers because the stabilizing effect of the surface tension does not prevail there. Note that the highest vapor depth has the strongest stabilizing effect in the system.

3.3. Effect of Vapor Depth on Evaporation Number

Evaporation number decreases while the vapor depth increases because of the stabilizing effect of the vapor depth. Figures 3.9 and 3.10 depict two values of heat source number, 0 and 4. Heat source number leads to a decrease in evaporation number and it can be noticed from Figure 3.10 that there is a saturation point for the evaporation number as it gradually decreases and reaches a saturation point.

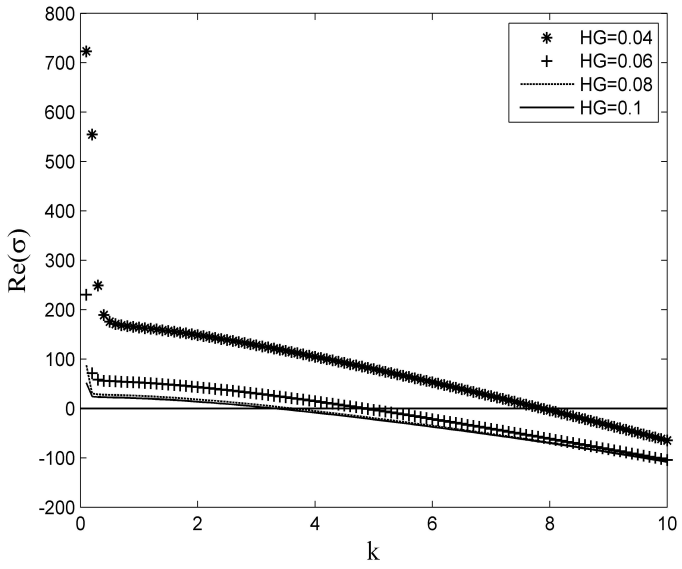

Figure 3.5. Dispersion curve to depict the effect of small vapor depth for $\phi = 1$ and $H_S = 1$.

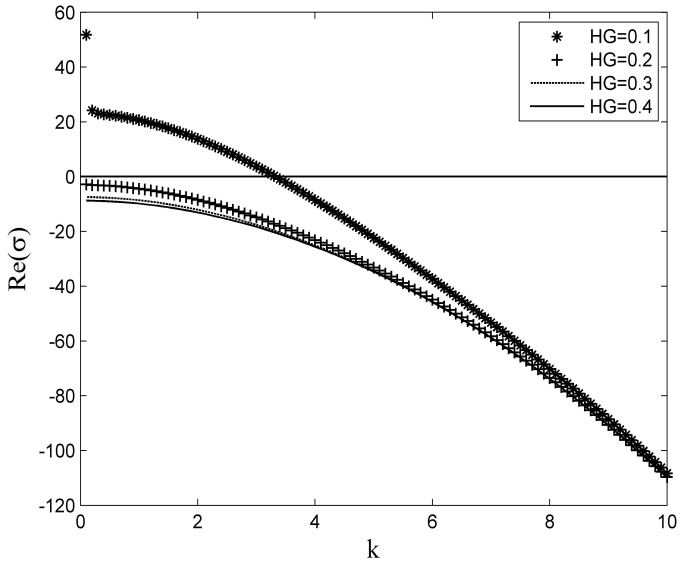

Figure 3.6. Dispersion curve to depict the effect of large vapor depth $\phi = 1$ and $H_S = 1$.

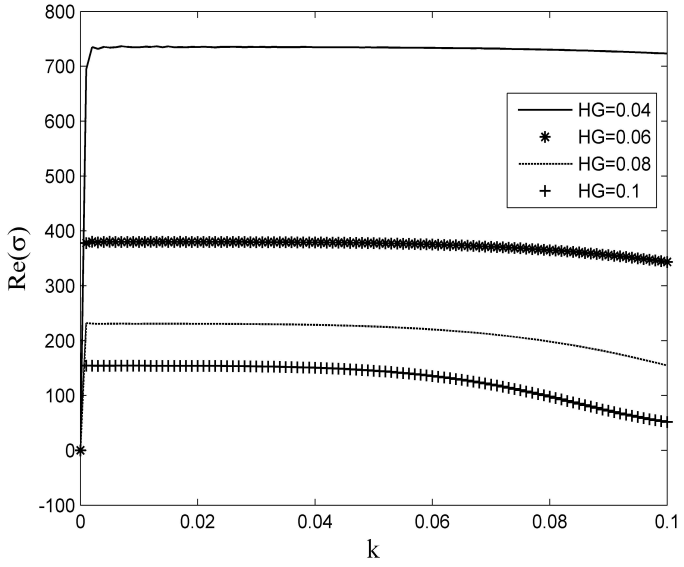

Figure 3.7. Dispersion curve versus wavenumber to depict the effect of small vapor depth for weak values of wave number for $\phi = 1$ and $H_S = 1$.

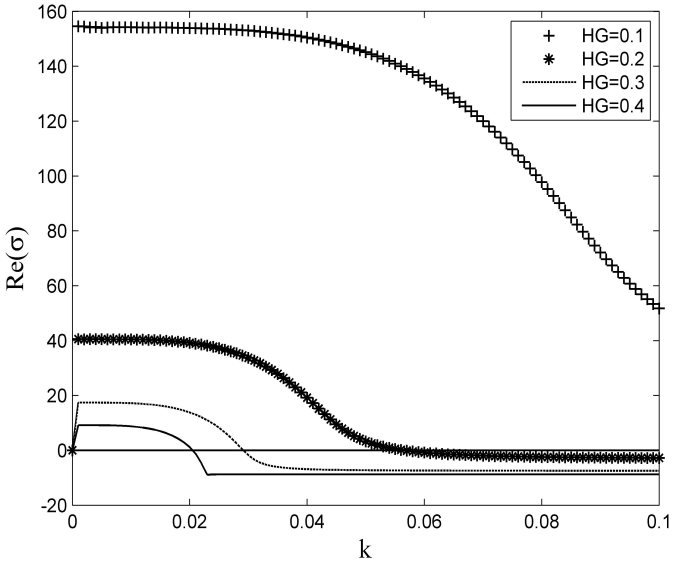

Figure 3.8. Dispersion curve versus wavenumber to depict the effect of large vapor depth for weak values of wave number for $\phi = 1$ and $H_S = 1$.

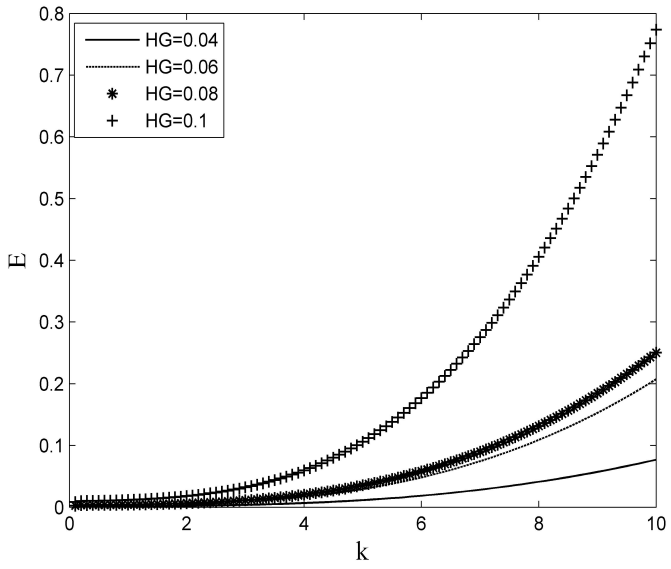

Figure 3.9. Effect of vapor depth on the critical evaporation number versus wave number for $\phi = 0$, $H_S = 1$, $H_G = 0.1$.

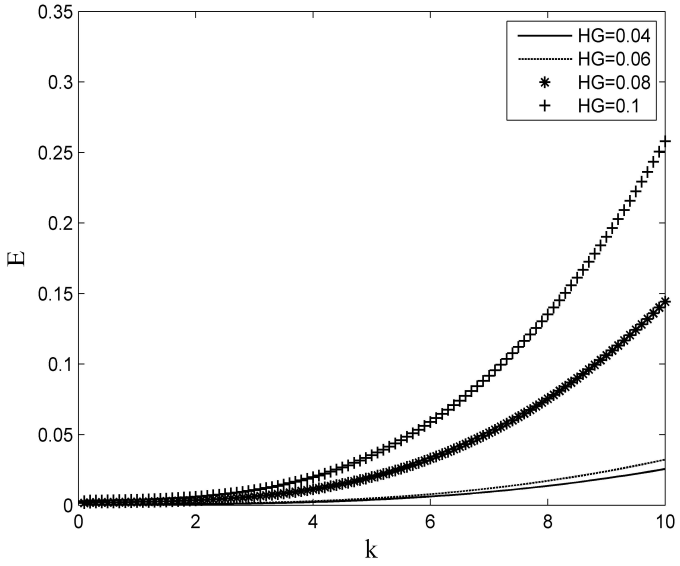

Figure 3.10. Effect of the vapor depth on the critical evaporation number versus wave number for $\phi = 4$, $H_S = 1$, $H_G = 0.1$.

3.4. Effect of Solid Depth on Dispersion Curve

Higher solid depth results in an increasing instability and this increment does not reach a saturation point. It can be seen from Figure 3.11 that the unstable behavior

of the system always increases with solid depth. Besides, it can be deduced from Figure 3.12 that small solid depths do not affect the system instability much. The dimensionless vapor depth and the heat source are 0.1 and 1, respectively.

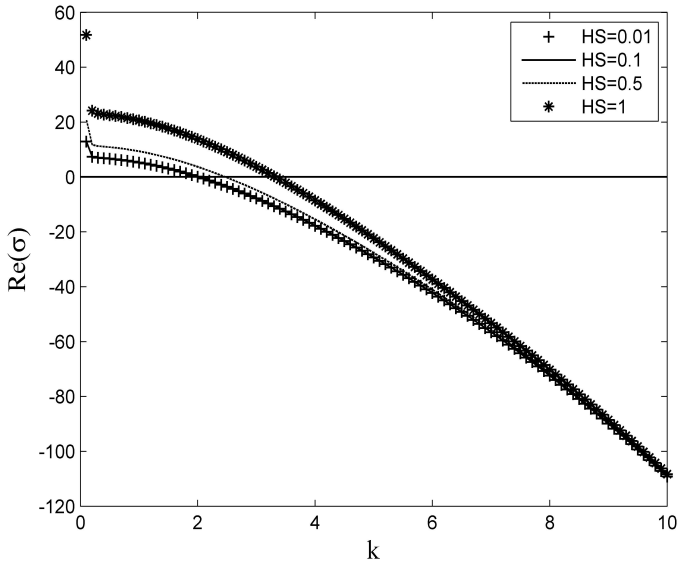

Figure 3.11. Dispersion curve to depict the effect of the solid depth for $\phi = 0$, $H_G = 0.1$.

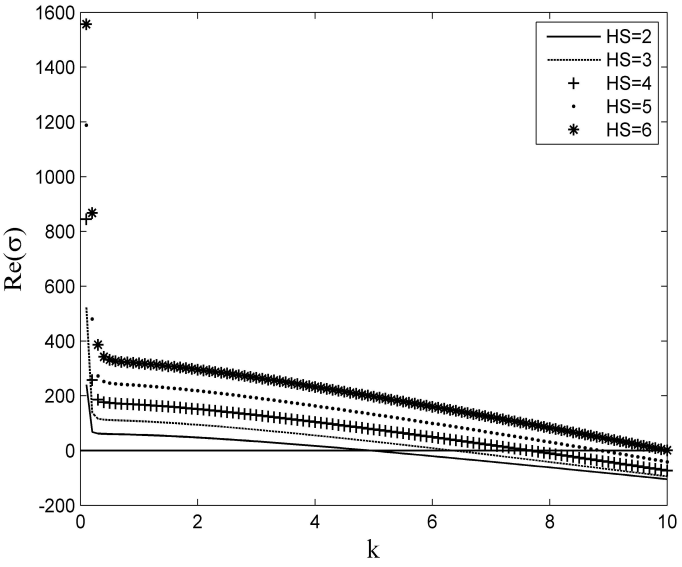

Figure 3.12. Dispersion curve to depict the effect of the solid depth for $\phi = 0$, $H_G = 0.1$.

Figure zooms on small wave numbers with various solid depths for the dispersion curve. Convergence could not be achieved for the dimensionless solid depths of 5 and 6.

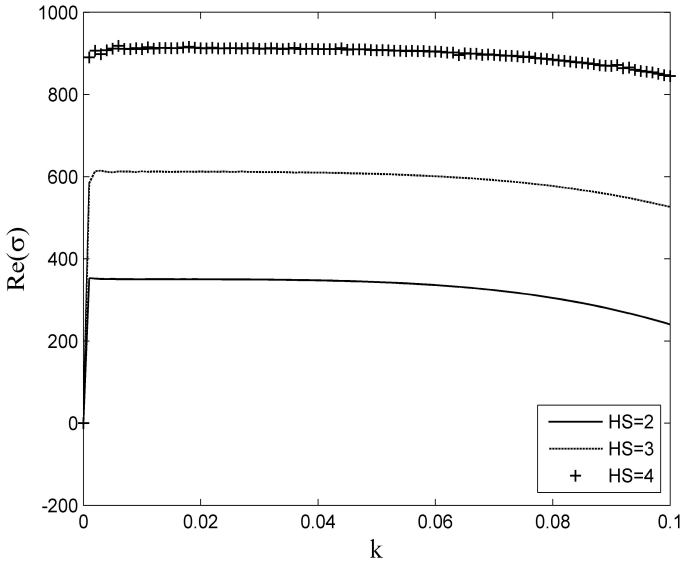

Figure 3.13. Dispersion curve to depict the effect of the solid depth for small wave numbers for $\phi = 0$, $H_G = 0.1$.

3.5. Effect of Solid Depth on Evaporation Number

In Figure 3.14, the dimensionless heat source is zero and as expected it is observed that zero value of the dimensionless heat source does not affect the instability of the system for different solid depths.

Figure 3.15 is acquired when the dimensionless heat source is taken as 1. In the presence of the heat source number, the evaporation number decreases as the solid depth becomes larger.

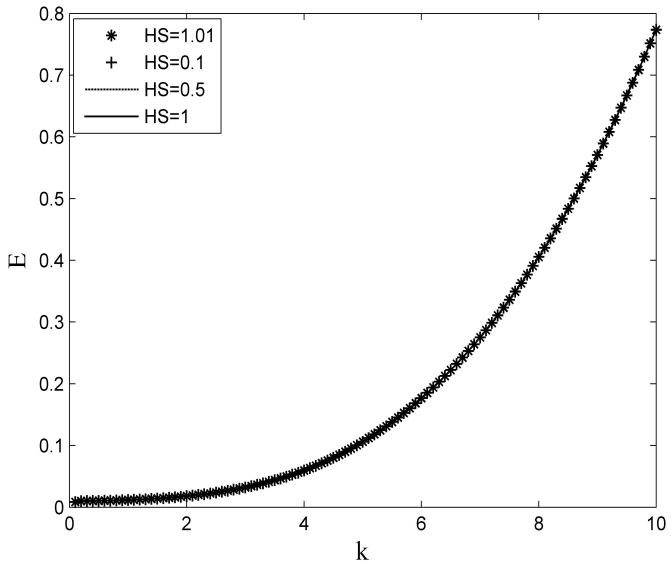

Figure 3.14. Critical evaporation number versus wavenumber for $\phi = 0$.

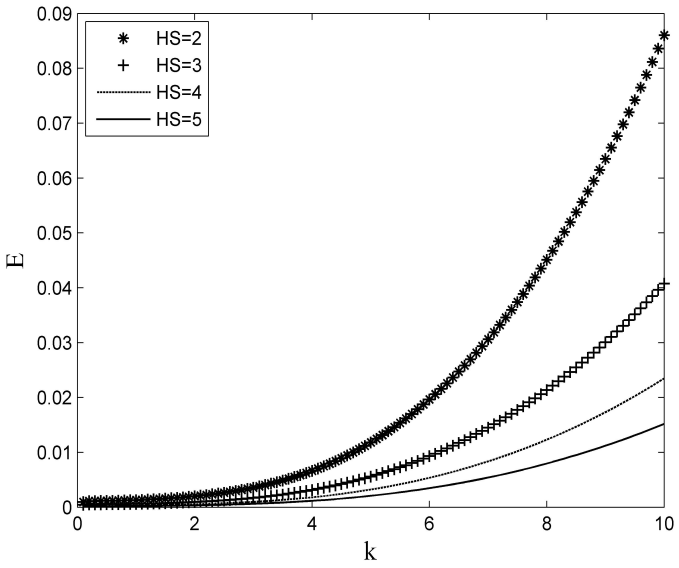

Figure 3.15. Critical evaporation number versus wavenumber for $\phi = 1$.

The effect of solid depth on the base state temperature profile was also investigated and it is presented in Figures 3.16 and 3.17. Now, the increase in temperature difference is higher than the previous case. The results can be verified by looking at the base state solution.

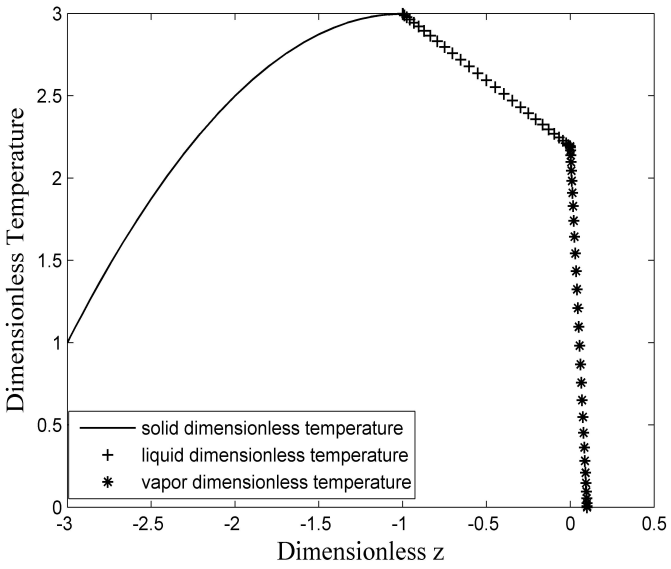

Figure 3.16. Dimensionless temperature versus dimensionless length for $H_S = 2$.

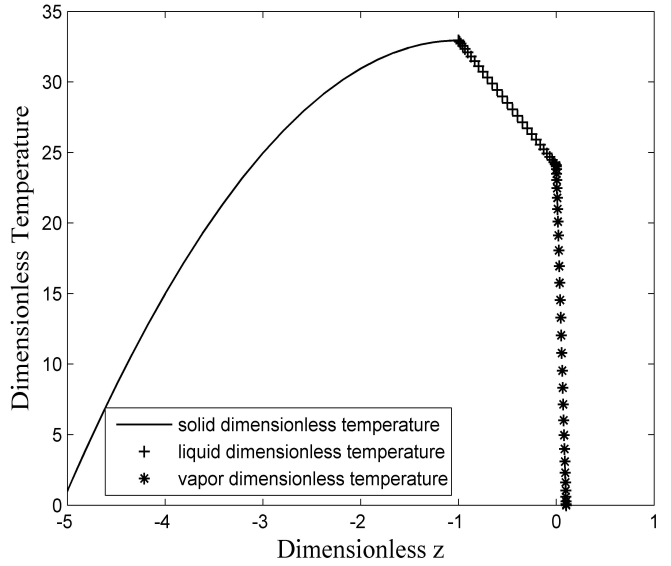

Figure 3.17. Dimensionless temperature versus dimensionless length for $H_S = 5$.

4. CONCLUSIONS

The aim of this study is to inquire into the effect of solid depth and heat source on the critical temperature difference at which convection starts for a solid-liquid-vapor system. In the study, it is conjectured that the physical parameters are constant and all the effects coming from the surface tension gradient and gravity are omitted; merely, the pure evaporation is considered. By using these assumptions, the mathematical model of the system is derived. Initially, the base state model which is the state of the system before convection commences is presented. The solely driving force in order to evaporate the system is the temperature difference. The other forces like concentration, surface tension gradient and gravity are not taken into consideration. Since the dimensionless heat source contains both the temperature difference and the heat flux, the ambit of their values relied on each other. After all, the normal mode expansion is performed in order to linearize the problem about the base state. The linear ordinary differential equations are solved by using Chebyshev spectral method which emanates from the method of weighted residuals.

The solid, the liquid and the vapor depths have impact on the stability of the system. An increase in the vapor depth results in a more stable system owing to thermal resistance and vapor dynamics. On the other hand, the liquid and the solid depths oppose to the effect of vapor depth on the stability of the system. Note that the effect of the liquid depth can be seen in the heat source number. Stability of the system decreases with the liquid and the solid depths. The effect of the liquid flow which is the reason for the instability strengthens with the depth. The reason for the instability with the solid depth is the base state solution. The base state solution is more comlex with respect to previous studies inasmuch as the solid part is added to the system. The base state solution involves the dimensionless heat source; therefore the interface temperature increases which also makes the system unstable.

For the future work, non-constant heat source can be used and this might bring an additional nonlinearity. Moreover, non-constant physical properties can be appended

to the study and the geometry of the system can be turned into a cylinder.

APPENDIX A: SURFACE VARIABLES

The surface is presented as:

$$f = z - Z(x,\, t) = 0 \tag{A.1}$$

The unit normal vector is acquired by dividing the gradient of f into its scalar value:

$$\mathbf{n} = \frac{\nabla f}{|\nabla f|} \tag{A.2}$$

Here:

$$\nabla f = \frac{\partial f}{\partial x}\mathbf{i} + \frac{\partial f}{\partial x}\mathbf{k} \tag{A.3}$$

The normal stress balance is read as:

$$\mathbf{n} = \frac{-\frac{\partial Z}{\partial x}\mathbf{i} + \mathbf{k}}{\left[1 + \left(\frac{\partial Z}{\partial x}\right)^2\right]^{\frac{1}{2}}} \tag{A.4}$$

The unit tangential vector is deduced by the same token using the relation of $\mathbf{n} \cdot \mathbf{t} = 0$:

$$\mathbf{t} = \frac{\mathbf{i} + \frac{\partial Z}{\partial x}\mathbf{k}}{\left[1 + \left(\frac{\partial Z}{\partial x}\right)^2\right]^{\frac{1}{2}}} \tag{A.5}$$

A surface is represented as:

$$f(\mathbf{r},\, t) = 0. \tag{A.6}$$

When the surface budges as Δs with time, Δt, in the direction of its normal, $f(\mathbf{r} \pm \Delta sn,\, t + \Delta t)$ is presented as:

$$f(\mathbf{r} \pm \Delta sn,\, t + \Delta t) = f(\mathbf{r},\, t) \pm \Delta sn.\nabla f(\mathbf{r},\, t) + \Delta t \frac{\partial f(\mathbf{r},\, t)}{\partial t} + ... \tag{A.7}$$

Eq. A.7 equals to Eq. A.6 as:

$$f(\mathbf{r} \pm \Delta sn,\, t + \Delta t) = f(\mathbf{r},\, t) = 0 \tag{A.8}$$

Then Eq. A.8 turns into:

$$\pm \Delta sn.\nabla f(\mathbf{r},\, t) = -\Delta t \frac{\partial f(\mathbf{r},\, t)}{\partial t} \tag{A.9}$$

The normal speed of the surface at the interface is read as:

$$u = \pm \frac{\Delta s}{\Delta t} = -\frac{\frac{\partial f(\mathbf{r},t)}{\partial t}}{\mathbf{n} \cdot v \nabla f(\mathbf{r},t)} \tag{A.10}$$

Eq. A.10 can be presented by using the unit normal as:

$$u = -\frac{\frac{\partial f}{\partial t}}{|\nabla f|} \tag{A.11}$$

Finally, the normal speed is read as:

$$u = \frac{\frac{\partial Z}{\partial t}}{\left[1 + \left(\frac{\partial Z}{\partial x}\right)^2\right]^{\frac{1}{2}}} \tag{A.12}$$

APPENDIX B: ENERGY BALANCE FOR A 1-D PURE SYSTEM

Energy balance in its frame variant form is read by:

$$\rho_L \left(\mathbf{v}_L - \mathbf{u}\right) \left\{ \left(\hat{U}_L - \hat{U}_G\right) + \frac{1}{2}\left(|\mathbf{v}_L|^2 - |\mathbf{v}_G|^2\right) \right\} \cdot \mathbf{n} + \left(\mathbf{q}_L - \mathbf{q}_G\right) \cdot \mathbf{n} - \left\{ \boldsymbol{T}_L \cdot \mathbf{v}_L - \boldsymbol{T}_G \cdot \mathbf{v}_G \right\} \cdot \mathbf{n} \quad \text{(B.1)}$$

The dot product of the stress balance with $\mathbf{u}$is taken as:

$$\left\{ \rho_L \left(\mathbf{v}_L - \mathbf{u}\right)\left(\mathbf{v}_L - \mathbf{v}_G\right) - \left(\boldsymbol{T}_L - \boldsymbol{T}_G\right) \right\} \cdot \mathbf{n} \cdot \mathbf{u} + \gamma 2H\mathbf{n} \cdot \mathbf{u} = \mathbf{0} \quad \text{(B.2)}$$

Eq. B.2 is subtracted from Eq. B.1 and the result is obtained as:

$$\rho_L \left(\mathbf{v}_L - \mathbf{u}\right) \left\{ \left(\hat{U}_L - \hat{U}_G\right) + \frac{1}{2}\left(|\mathbf{v}_L|^2 - |\mathbf{v}_G|^2\right) - \left(\mathbf{v}_L - \mathbf{v}_G\right) \cdot \mathbf{u} \right\} \cdot \mathbf{n} + \left(\mathbf{q}_L - \mathbf{q}_G\right) \cdot \mathbf{n} - \left\{ \boldsymbol{T}_L \cdot \left(\mathbf{v}_L - \mathbf{u}\right) - \boldsymbol{T}_G \cdot \left(\mathbf{v}_G - \mathbf{u}\right) \right\} \cdot \mathbf{n} = 0 \quad \text{(B.3)}$$

The following relation is used to get rid of the terms which make Eq. B.3 look frame variant:

$$\frac{1}{2}\left(\mathbf{v}_L - \mathbf{u}\right) \cdot \left(\mathbf{v}_L - \mathbf{u}\right) = \frac{1}{2}|\mathbf{v}_L|^2 - \mathbf{v}_L \cdot \mathbf{u} + \frac{1}{2}|\mathbf{u}|^2 \quad \text{(B.4)}$$

$$\frac{1}{2}|\mathbf{v}_L|^2 = \frac{1}{2}\left(\mathbf{v}_L - \mathbf{u}\right)^2 + \mathbf{v}_L \cdot \mathbf{u} - \frac{1}{2}|\mathbf{u}|^2 \quad \text{(B.5)}$$

$$\frac{1}{2}\left(|\mathbf{v}_L|^2 - |\mathbf{v}_G|^2\right) = \frac{1}{2}\left(\mathbf{v}_L - \mathbf{u}\right)^2 + \mathbf{v}_L \cdot \mathbf{u} - \frac{1}{2}|\mathbf{u}|^2 - \frac{1}{2}\left(\mathbf{v}_G - \mathbf{u}\right)^2 - \mathbf{v}_G \cdot \mathbf{u} + \frac{1}{2}|\mathbf{u}|^2 \quad \text{(B.6)}$$

$$\frac{1}{2}\left(|\mathbf{v}_L|^2 - |\mathbf{v}_G|^2\right) = \frac{1}{2}\left\{(\mathbf{v}_L - \mathbf{u})^2 - (\mathbf{v}_G - \mathbf{u})^2\right\} + (\mathbf{v}_L - \mathbf{v}_G)\cdot\mathbf{u} \tag{B.7}$$

Eq. B.7 is inserted into Eq. B.3 and the result is:

$$\rho_L(\mathbf{v}_L - \mathbf{u})\left\{\left(\hat{U}_L - \hat{U}_G\right) + \frac{1}{2}\left((\mathbf{v}_L - \mathbf{u})^2 - (\mathbf{v}_G - \mathbf{u})^2\right)\right\}\cdot\mathbf{n} + (\mathbf{q}_L - \mathbf{q}_G)\cdot\mathbf{n} - \{\boldsymbol{T}_L\cdot(\mathbf{v}_L - \mathbf{u}) - \boldsymbol{T}_G\cdot(\mathbf{v}_G - \mathbf{u})\}\cdot\mathbf{n} = \mathbf{0} \tag{B.8}$$

The following equations are used for the stress tensor and the internal energy.

$$\boldsymbol{T} = -p\boldsymbol{I} + \boldsymbol{S} \tag{B.9}$$

$$\hat{U} = \hat{H} - \frac{p}{\rho} \tag{B.10}$$

Lastly, energy balance equation is acquired as:

$$\rho_L(\mathbf{v}_L - \mathbf{u})\left\{\left(\hat{H}_L - \hat{H}_G\right) + \frac{1}{2}\left((\mathbf{v}_L - \mathbf{u})^2 - (\mathbf{v}_G - \mathbf{u})^2\right)\right\}\cdot\mathbf{n} + (\mathbf{q}_L - \mathbf{q}_G)\cdot\mathbf{n} + \{\boldsymbol{S}_L(\mathbf{v}_L - \mathbf{u}) - \boldsymbol{S}_G\cdot(\mathbf{v}_G - \mathbf{u})\}\cdot\mathbf{n} = \mathbf{0} \tag{B.11}$$

APPENDIX C: THERMODYNAMIC EQUILIBRIUM AT THE INTERFACE

The thermodynamic equilibrium at the interface is described by:

$$\hat{G}_L = \hat{G}_V \tag{C.1}$$

Here, $\hat{G}_L$ and $\hat{G}_G$ are the liquid and vapor Gibbs free energies per unit mass, respectively. Surface can be in any shape; therefore Eq. C.1 is now represented as:

$$\hat{G}_{L_{CURVED}} = \hat{G}_{G_{CURVED}} \tag{C.2}$$

and

$$\hat{G}_{L_{FLAT}} = \hat{G}_{G_{FLAT}} \tag{C.3}$$

The following equation is acquired from Eq. C.2 and C.3 as:

$$\left(\hat{G}_{L_{CURVED}} - \hat{G}_{L_{FLAT}}\right) - \left(\hat{G}_{G_{CURVED}} - \hat{G}_{G_{FLAT}}\right) = 0 \tag{C.4}$$

The definition of the Gibbs free energy is:

$$d\hat{G} = -\hat{S}dT + \hat{V}dP \tag{C.5}$$

Here, $\hat{S}$ and $\hat{V}$ denotes the entropy and the volume per unit mass, respectively. If the change in the entropy and the volume per unit mass with the temperature and the pressure does not affect significantly, Eq. C.5 becomes:

$$\left(\hat{S}_G - \hat{S}_L\right) dT - \frac{1}{\rho_G} dP_G = 0 \tag{C.6}$$

Also Eq. C.7 equals to zero:

$$\left(\hat{G}_G - \hat{G}_L\right) = \left(\hat{H}_G - \hat{H}_L\right) - \left(\hat{S}_G - \hat{S}_L\right) T \tag{C.7}$$

Eq. C.7 is inserted into Eq. C.6 for the entropy per unit mass:

$$\frac{\hat{H}_G - \hat{H}_L}{T} dT + \hat{V}_L dP_L - \frac{RT}{P_G} dP_G = 0 \tag{C.8}$$

Latent heat of evaporation is defined as:

$$\mathcal{L} = \hat{H}_G - \hat{H}_L \tag{C.9}$$

Eq. C.9 is inserted into Eq. C.8 and it is integrated as:

$$\int_{T_{FLAT}}^{T_{CURVED}} \frac{\mathcal{L}}{T^2} dT + \int_{P_{L_{FLAT}}}^{P_{L_{CURVED}}} \frac{\hat{V}_L}{T} dP_L - \int_{P_{G_{FLAT}}}^{P_{G_{CURVED}}} \frac{R}{P_G} dP_G = 0 \tag{C.10}$$

$$\mathcal{L}\left(\frac{1}{T_{curved}} - \frac{1}{T_{flat}}\right) + \frac{\hat{V}_L}{T}\left(\frac{1}{P_{L_{CURVED}}} - \frac{1}{P_{L_{FLAT}}}\right) - R\left(lnP_{G_{CURVED}} - lnP_{G_{FLAT}}\right) = 0 \tag{C.11}$$

Pressure variation in the liquid phase can be omitted; hence Eq. C.11 can be read as:

$$\mathcal{L}\left(\frac{1}{T_{curved}} - \frac{1}{T_{flat}}\right) - R\left(lnP_{G_{CURVED}} - lnP_{G_{FLAT}}\right) = 0 \tag{C.12}$$

REFERENCES

1. Ozen, O., *Effect of Vapor Dynamics on Interfacial Instabilities*, Ph.D. Thesis, University of Florida, 2004.

2. Uguz, K. E., *Evaporative Instability in Binary Mixtures*, Ph.D. Thesis, University of Florida, 2012.

3. Burelbach, J. P., S. G. Bankoff, and S. H. Davis, "Nonlinear Stability of Evaporating/Condensing Liquid Films", *Journal of Fluid Mechanics*, Vol. 195, pp. 463-494, 1988.

4. Oron, A., "Nonlinear Dynamics of Thin Evaporating Liquid Films Subject to Internal Heat Generation", *Fluid Dynamics at Interfaces*, pp. 3-15, 1999.

5. Margerit, J., M. Dondlinger, and P.C. Dauby, "Improved 1.5-Sided Model for the Weakly Nonlinear Study of Bénard-Marangoni Instabilities in an Evaporating Liquid Layer", *Journal of Colloid and Interface Science*, Vol. 290, pp. 220-230, 2005.

6. Pearson, J. R. A., "On Convection Cells Induced by Surface Tension", *Journal of Fluid Mechanics*, Vol. 4, pp. 489-500, 1958.

7. Haut, B., and, P. Colinet, "Surface-Tension-Driven Instabilities of a Pure Liquid Layer Evaporating into an Inert Gas", *Journal of Colloid Interface Science*, Vol. 285, pp. 296-305, 2005.

8. Ozen, O., and, R. Narayanan, "The Physics of Evaporative and Convective Instabilities in Bilayer Systems: Linear Theory", *Physics of Fluids*, Vol. 16, pp. 4644-4652, 2004.

9. McFadden, G. B., S. R. Coriell, K. F. Gurski, and D. L. Cotrellc, "Onset of Convection in Two Liquid Layers with Phase Change", *Physics of Fluids*, Vol. 19, pp.

104109-13, 2007.

10. Huang A., and D. D. Joseph, "Instability of the Equilibrium of a Liquid Below Its Vapour Between Horizontal Heated Plates", *Journal of Fluid Mechanics*, Vol. 242, pp. 235-247, 1992.

11. Shankar, P., and M. Deshpande, "On the Temperature Distribution in Liquid Vapor Phase Change Between Plane Liquid Surfaces", *Physics of Fluids*, Vol. A 2, pp. 1030-1038, 1990.

12. Plesset, M. S., "Note on the Flow of Vapor Between Liquid Surfaces", Journal of Chemical Physics, Vol. 20, pp. 790, 1952.

13. Margerit, J., P. Colinet, G. Lebon, C. S. Iorio, and J. C. Legros, "Interfacial Nonequilibrium and Benard-Marangoni Instability of a Liquid-Vapor System", *Physical Review*, Vol. E 68, pp. 041601-14, 2003.

14. Ward, C., and D. Stanga, "Interfacial Conditions During Evaporation or Condensation of Water", *Physical Review*, Vol. E 64, pp. 051509-9, 2001.

15. Guo, W., and R. Narayanan, "Interfacial Instability Due to Evaporation and Convection: Linear and Nonlinear Analyses", *Journal of Fluid Mechanics*, Vol. 650, pp. 363-389, 2010.

16. Johns, L. E., and R. Narayanan, *Interfacial Instability*, Springer-Verlag, New York, 2002.

17. Guo, W., G. Labrosse, and R. Narayanan, *The Chebyshev Spectral Method in Transport Phenomena*, Springer-Verlag, New York, 2012.

18. Ozen, O., and R. Narayanan, "Comparison of Evaporative Instability with Marangoni Instability", *Physics of Fluids*, Vol. 44, pp. 1342-1348, 2004.